Environmental Science
Processes & Impacts

PAPER

View Article Online
View Journal | View Issue

Cite this: *Environ. Sci.: Processes Impacts*, 2019, **21**, 63

Microphysics of the aqueous bulk counters the water activity driven rate acceleration of bromide oxidation by ozone from 289–245 K†

Jacinta Edebeli,[ab] Markus Ammann [a] and Thorsten Bartels-Rausch *[a]

The reaction of ozone with bromide is an initiation process in bromine activation resulting in the formation of reactive bromine species with impacts on the fate of compounds in the lower atmosphere. Environmental halide sources often contain organics, which are known to influence aqueous bulk reactivity. Here, we present a study investigating the temperature dependence of bromide oxidation by ozone using a coated wall flow tube reactor coated with an aqueous mixture of citric acid, as a proxy for oxidized secondary organic matter, and sodium bromide. Using the resistor model formulation, we quantify changes in the properties of the aqueous bulk relevant for the observed reactivity. The reactive uptake coefficient decreased from 2×10^{-6} at 289 K to 0.5×10^{-6} at 245 K. Our analysis indicates that the humidity-driven increase in concentration with a corresponding increase in the *pseudo*-first order reaction rate was countered by the colligative change in ozone solubility and the effect of the organic fraction *via* increased viscosity and decreased diffusivity of ozone as the temperature decreased. From our parameterization, we provide an extension of the temperature dependence of the reaction rate coefficients driving the oxidation of bromide, and assess the temperature-dependent *salting* effects of citric acid on ozone solubility. This study shows the effects of the organic species at relatively mild temperatures, between the freezing point and eutectic temperature of sea as is typical for the Earth's cryosphere. Thus, this study may be relevant for atmospheric models at different scales describing halogen activation in the marine boundary layer or free troposphere including matrices such as sea-spray aerosol and brine in sea ice, snow, and around mid-latitude salt lakes.

Received 7th September 2018
Accepted 7th November 2018

DOI: 10.1039/c8em00417j

rsc.li/espi

Environmental significance

Tropospheric halide oxidation by ozone is a prevalent process in regions of the world containing halide sources such as polar regions and around salt lakes. This process has significant implications on the tropospheric ozone budget and on the fate of compounds such as elemental mercury in the marine boundary layer. This study investigated the oxidation of bromide by ozone in a medium containing an organic species representative of secondary organic matter from 16 °C to −25 °C. Our results indicate that the presence of the organic species counters the rate acceleration associated with decreasing water activity with decreasing temperature due to effects on the viscosity of the medium and solubility of ozone in the medium.

Introduction

The reaction of ozone (O_3) with halides producing reactive halogen species (RHS) in the troposphere is an important chemical process with implications for the oxidation capacity of the atmosphere and the fate of compounds in the atmosphere.[1–3] Of importance is the reaction between RHS and gas phase mercury resulting in increased mercury deposition, which has implications on human and ecosystem health.[1,2,4] While all halides may be involved, with respect to sea ice and sea spray aerosols, bromide may dominate due to its relative abundance and high reactivity compared to other halides.[1,3,5]

Studies show that aerosols containing halides such as sea spray aerosols significantly contribute to global halogen chemistry *via* multiphase chemistry on and within aerosol particles.[6–9] Sea-spray aerosol is also partly responsible for the salinity of surface snow[3,10] resulting from scavenging and deposition along with snow fall onto polar and alpine snow packs. Field and satellite measurements have identified local, regional, and global scale effects of atmospheric halogen chemistry on O_3 and on the mercury cycle.[8,9] However, there are still uncertainties in the mechanism of halide oxidation by ozone especially in less understood complex sources such as aerosols or snow containing mixtures of organics and salts.[6,7]

[a]*Laboratory of Environmental Chemistry, Paul Scherrer Institut, Villigen PSI, Switzerland. E-mail: thorsten.bartels-rausch@psi.ch*

[b]*Swiss Federal Institute of Technology, ETH Zurich, Zurich, Switzerland*

† Electronic supplementary information (ESI) available. See DOI: 10.1039/c8em00417j

While the microphysics of aqueous aerosol particles is reasonably well understood, in complex environments such as snow and sea-ice, the structural arrangement of the non-frozen aqueous phase is less obvious. It may be expected that the water activity is controlled by the presence of ice.[3,5,11] The concentration of aqueous solutes in equilibrium with ice depends on temperature and follows the phase diagram of the aqueous mixtures.[5,12] Below the freezing point of ice, as the temperature decreases, the water activity in solution decreases until the eutectic point is reached (Fig. 1). The activity of the solutes increases similarly to the so-called "freeze concentration effect" described by Takenaka and Watson.[13] When the concentration of the solutes in the unfrozen aqueous phase exceeds the solubility limit of a solute, precipitation of that solute may occur.[3] In sea-ice formation, sodium chloride (NaCl) precipitates out at a warmer temperature than bromide leading to an enrichment of bromide relative to NaCl.[3] Fig. 1 gives an example and shows how the equilibrium mass fraction of sodium bromide (NaBr) in aqueous solution increases during freezing.[14] The environmental impact of this increase in the concentration of solutes with decreasing temperature has been discussed[5] and may include the formation of products not typically formed at lower concentrations.[15]

Investigations of the composition of sea-spray aerosol show a significant organic component, which may be up to 50% of the aerosol mass.[16] The organic fraction plays a role in the properties of the aerosol, such as hygroscopic properties and viscosity.[17–19] Indeed, investigations of halide oxidation in organic acid–halide mixtures indicate the effects of the organic fraction on the uptake of O_3.[20] These studies show that in addition to providing acidity (which catalyses the reaction), the acids may affect the prevalence of the surface reaction[20] and the propensity of halide ions for the interface.[21,22] Regarding the physical properties of organic containing solutions, studies show that the viscosity of organic solutions may reduce bulk reactivity by decreasing the diffusivity of the reactive solute (in this case, O_3).[23–25]

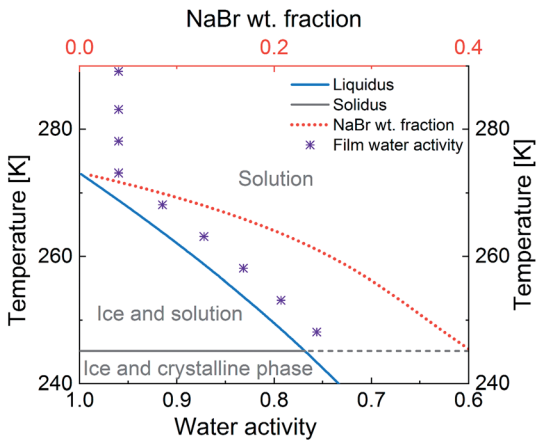

Fig. 1 Representation of the phase diagram of a NaBr–water binary solution (lines) and of the water activity in the film of study (Purple '*') as a function of water activity and temperature. The blue line denotes the solid–liquid equilibrium curve of ice; the red dot line is the weight fraction of NaBr in solution in equilibrium with ice; the grey line indicates the eutectic temperature, where NaBr crystallises.[14] Water activity = relative humidity with respect to liquid water (%)/100.

Thus, the organic fraction of sea-spray aerosols, though not considered in atmospheric chemistry models, may impact the observed multiphase halogen activation, both during long range transport of sea spray aerosol in the troposphere and in snow or on sea-ice after deposition. Environmental ice compartments, such as sea ice and snow also contain halides and can partake in halide oxidation.[26–29] Just like inorganic salts, organics may also be excluded to the brine pockets during freezing and may similarly affect the properties of the unfrozen aqueous phase in snow and environmental ice.[30] These effects, in particular the influence of viscosity on reactivity, usually require rather low relative humidity as is typically found in the free troposphere. Here we focus on these effects of an organic acid on the chemical reactivity at moderate humidity as is typical for the snow covered boundary layer and the interstitial air in snow.

The reaction between O_3 in the gas phase and bromide in the condensed phase of aerosols, sea ice, and snow is one initiation process for the formation of reactive bromine species. This is a multiphase reaction, which can occur in the dark, leading to the production of photo-labile bromine (Br_2; R1–R5) with R2 and R3 as the rate limiting steps.[31–34] Br_2 produced during the night or during the polar winter may serve as a reservoir for daytime or polar spring photolytic halogen activation.[4,35] Reactions R4 and R5 may also involve chloride and/or iodide leading to the production of reactive inter-halogen species (*e.g.* IBr, BrCl).[36,37] Production of inter-halogen species, especially BrCl, may also depend on the relative abundance of the respective halides.[38]

Here, we focus on the reaction of bromide with ozone in the dark. Kinetic studies on bromide (Br^-) oxidation by O_3 indicate a multiphase process with a significant interfacial component.[39–41] Aqueous bulk bromide oxidation by ozone is relatively slow with a rate coefficient of $\sim$258 M^{-1} s^{-1} at 298 K.[32] Hunt *et al.* showed that the observed Br_2 production resulting from this reaction system exceeded that expected from bulk aqueous production alone, and suggested a contribution from interfacial processes.[39] Other studies probing possibilities of additional interfacial processes corroborate this suggestion by Hunt *et al.*[40–43] Oldridge and Abbatt, while monitoring Br_2 production, showed that the interfacial processes become significant at atmospherically relevant low ozone concentrations.[40]

Studies on the interfacial process indicate that this process proceeds *via* the formation of an adsorbed intermediate species on the surface of the observed system.[39] Artiglia *et al.* recently observed this intermediate, the bromide ozonide, $BrOOO^-$, and showed that it is surface active and stabilized by water molecules on the surface.[41] The mechanism of formation and the role of this intermediate has also been studied by theoretical calculations.[44] Gladich *et al.*, in their theoretical study of this reaction, showed that *via* intersystem crossing of $BrOOO^-$ from the singlet state to triplet state, this Br^- oxidation process can proceed successfully in the dark.[44]

Often, studies investigate halide oxidation in salt solutions only. In addition, though research has concentrated mostly on halogen chemistry with O_3 in polar regions, similar halogen activation has been observed in warmer environments.[40,45]

Temperature influences properties such as solubility, viscosity, and reaction rates with implications on the observed reactive loss of O_3.

$$Br^- + O_3 \underset{k_{-1}}{\overset{k_1}{\rightleftharpoons}} BrOOO^- \quad (R1)$$

$$BrOOO^- + H^+ \xrightarrow{k_2} HOBr + O_2 \quad (R2)$$

$$BrOOO^- + H_2O \xrightarrow{k_3} HOBr + O_2 + OH^- \quad (R3)$$

$$HOBr + Br^- + H^+ \overset{\text{fast}}{\rightleftharpoons} Br_2 + H_2O \quad (R4)$$

$$Br_2 + Br^- \overset{\text{fast}}{\rightleftharpoons} Br_3^- \quad (R5)$$

Therefore, there are two objectives for the study presented herein. The first objective is to measure the uptake of O_3 *via* reaction with bromide in a mixture containing citric acid (CA) and NaBr in water, over a wide temperature (T) range (−25 °C to 16 °C). CA was chosen to be a proxy for oxidised organic material representative of aged primary or secondary organic material abundant in marine environments. Experiments were conducted using thin films (equilibrated to experimental conditions) of the mixture in a temperature-regulated coated wall flow tube setup. An essential requirement of the experimental design was to avoid freezing while staying close to the ice-*liquidus* line in the NaBr–water–organic ternary solution at temperatures below 0 °C (Fig. 1). This was achieved by maintaining a relative humidity of about 96% with respect to water vapour pressure over ice (RH_{ice}) in the setup at temperatures below 0 °C and a relative humidity of 96% above 0 °C (RH_{water}).[46,47] This means that the relative humidity with respect to liquid water (RH_{water}) ranged from 96% at 16 °C to 75% at −25 °C.[46,47] Thus, the $RH_{water} - T$ space covered in this study is directly relevant for atmospheric aerosol trajectories, but also remains close, in terms of water activity, to the conditions of liquid phases in equilibrium with ice, such as within snow or sea ice. As such, it allows for covering a significant temperature range without the complications related to ice formation.

The second objective is to extensively assess the influence of temperature-induced changes in the system on the observed uptake coefficients of O_3 *via* temperature-dependent variables controlling the microphysics and kinetics.[5,23,48] Using the resistor model formulation,[50,51] we attempt to describe the changes in reactant concentration, diffusivity, and pH to provide information on how these potentially opposing effects influence the observed temperature-dependent O_3 uptake. Development of the parameterization used in this study focuses on the properties and reactivity in the aqueous bulk.

Experimental

Materials and methods

The experimental work in this study was conducted using a temperature-regulated coated wall flow tube setup at atmospheric pressure (ESI Fig. S1†). The setup is fitted with a temperature-regulated injector for dosing humidified O_3 (and other gases) into the coated flow tube. This study was conducted using sodium bromide (NaBr, Sigma Aldrich, >99.0%), citric acid monohydrate (CA, Sigma Aldrich >99.0%), and ultrapure water (18 MΩ cm).

Tube preparation. A 50 cm long flow tube with an internal diameter of 1.2 cm was coated with a NaBr (0.34 M) and citric acid (0.31 M) mixture in 400 μL water (pH = 1.60 ± 0.02). Before coating, the tube was etched with 5% hydrofluoric acid (HF) and rinsed thoroughly with deionized water until the pH of the water in the tube was near neutral. The tube was then dried and coated with the solution under a N_2 flow at 55% relative humidity (RH_{water}) and room temperature. No crystal formation was observed during this process. The coated tube was conditioned at the experimental temperature and RH_{water} (see Fig. 1) with a flow of humidified synthetic air for an hour before exposure to O_3. Gases were delivered to the flow tube *via* the injector.

Ozone exposure. O_3 was generated from oxygen (at a flow rate of 200 ml min^{-1} at standard temperature and pressure (STP)) using a Hg penray UV lamp. The generated O_3 stream was humidified by adding a flow of humidified nitrogen gas (780 ml min^{-1}). The coated flow tube was exposed to humidified O_3 in O_2/N_2 in 15 minute cycles between the flow tube and a bypass (to measure the maximum O_3 and check for fluctuations in the O_3 delivered to the flow tube). The O_3 concentration in parts per billion by volume (ppb) was measured using a commercial O_3 analyser (Teledyne, model 400E).

Experiments were conducted from −25 °C to 16 °C. At each temperature, a cycle between the bypass and the flow tube was repeated at least three times with an exposure length of 25 cm (exposed surface area of 94.3 cm^2). Ozone concentrations were also measured at 0 cm (just outside the tube) to account for losses that were not from the coated part of the flow tube (<1%). The ozone concentration was also measured as a function of injector position, and thus length of the coated flow tube, exposed at 5 °C and −5 °C to confirm the first order kinetics for our analyses (ESI Fig. S2†). At least one independent repeat was conducted on a different day for each temperature. O_3 loss was also measured at different O_3 concentrations at some temperatures (0 °C, −10 °C, −20 °C, and −25 °C).

Viscosity measurement. The equilibrium concentration in the film at each temperature was calculated using the AIOMFAC model version 2.18.[49] We measured the viscosity of the equilibrium compositions using a Thermo-Scientific Haake Viscotester iQ Air. Viscosity was measured at the experimental temperature and relative humidity using plate geometry. The relative humidity in the viscosity measurement cell was controlled with a flow of humidified N_2 (200 ml min^{-1}). The samples were allowed to equilibrate at the set temperature and relative humidity for 10 to 15 minutes before measurement.

Data analyses

Uptake coefficients: observed uptake coefficients (γ_{obs}). We determined the uptake coefficient of O_3 in the system from observing the change in O_3 concentration due to exposure to the

coated flow tube. Fig. 2 shows a sample of the raw data obtained from the O_3 analyser at 5 °C during ozone exposure to the coated flow tube. Uptake coefficients (γ_{obs}) were calculated with the average O_3 concentration through the bypass ($[O_3]_{bypass}$) before and after the flow tube exposure, and through the flow tube ($[O_3]_{flow\ tube}$) in ppb for each cycle using eqn (1) below. The uptake coefficient is defined as the probability that a collision of an O_3 molecule with the coated wall will result in O_3 loss.[40,50,51] These coefficients provide the "normalized sum of" losses, which is a combination of all processes involved in the removal of ozone. The average O_3 uptake coefficient of the three cycles between the bypass and the flow tube per repeat is taken as the mean uptake coefficient for that experiment. γ_{obs} was corrected for gas phase diffusion limitation following the Cooney–Kim–Davis (CKD) method[52] (see ESI† for details).

$$\gamma_{obs} = \frac{4\varphi \times \left[\ln\left(\frac{[O_3]_{bypass}}{[O_3]_{flowtube}}\right)\right]}{\omega_{O_3} \times SA} \times C_{gd} \quad (1)$$

$$\omega_{O_3} = \sqrt{\frac{8RT}{\pi M_{wO_3}}} \quad (2)$$

where φ is the flow rate of O_3 through the flow tube (980 ml min^{-1}); ω is the mean thermal velocity of O_3 in the gaseous phase, cms^{-1};[53] SA is the exposed internal surface area of the tube, 94.3 cm^2; M_{wO_3} is the molecular weight of O_3; C_{gd} is the diffusion correction factor.

Uptake coefficients: parameterization of uptake coefficients. The uptake coefficient is a combination of surface and bulk uptake processes, and is often evaluated using a resistance model method.[50,51] This method describes the uptake coefficient as a convolution of serial and parallel processes (expressed as resistances) under steady state conditions. Uptake starts with the accommodation of O_3 on the surface by collision from the gas phase, from where it may undergo reaction with other species on the surface, desorb back to the gas phase or enter into the bulk of the solution, diffuse, and react there. The resistance model is a representation of the complete solutions to the coupled differential equations describing these processes under steady state conditions analogous to electrical resistances of parallel or serial processes.

In this study, we assume that accommodation on the surface (preceding the surface reaction described by Γ_{surf} and also preceding the surface to bulk transfer) is not rate limiting. We also assume that the surface to bulk transfer of O_3 is not rate limiting, as justified further below. Thus, within these assumptions, the surface reaction operates independently of and parallel to diffusion and reaction in the bulk. Hence, the total uptake can be represented by the sum of the inverse resistances for diffusion and reaction in the bulk (Γ_{bulk}) and for the surface reaction (Γ_{surf}) (eqn (3)). By themselves, Γ_{bulk} and Γ_{surf} are reaction rates normalized to the gas kinetic collision if they would be the only limiting processes.

$$\gamma_{calc} = \Gamma_{surf} + \Gamma_{bulk}, \quad (3)$$

where

$$\Gamma_{surf} = \frac{4\ k_s K N_{max}}{\omega_{O_3}\left(1 + K[O_3]_g\right)} \quad (4)$$

and

$$\Gamma_{bulk} = \frac{4HRT \times \sqrt{D_{O_{3l}} \times k_b^I}}{\omega_{O_3}} \quad (5)$$

The reactive surface uptake (Γ_{surf}) calculated using eqn (4)[50] represents a "Langmuir–Hinshelwood-type" surface reaction mechanism,[40] in which "Langmuir-type" adsorption precedes reaction. Partitioning of the reactive gas to the surface from the gas phase is described by the equilibrium constant, K, such that $K \times [O_3]_g/(1 + K \times [O_3]_g)$ is the fractional surface coverage.[40] Artiglia *et al.* have recently shown that the Langmuir equilibrium constant, K, and the maximum surface coverage, N_{max}, in eqn (4) are linked to the equilibrium and maximum coverage of the reaction intermediate, a bromide ozonide, at the surface, when describing the oxidation of bromide. Here, we used the same approach and set N_{max} to 10^{12} molecules per cm^2, the saturation surface concentration of the bromide ozonide intermediate as reported by Artiglia *et al.* The apparent equilibrium partitioning coefficient K represents a lumped parameter describing the equilibrium between gas-phase ozone and the surface concentration of the ozonide and was set to ($K = 6 \times 10^{-13}\ \exp(686/T^{-1})$) cm^3 per molecule. The surface reaction rate coefficient is denoted as k_s and was set to $2.1 \times 10^{12}\ \exp\left(\frac{-76\ 400}{RT}\right)$ s^{-1}.[41] We note that the transfer of O_3 into the bulk aqueous phase also first involves the adsorption of O_3 to the surface, in parallel to and independently of the formation of the bromide ozonide. Given the fairly low bromide concentrations, the surface is still largely dominated by water molecules. The adsorption equilibrium constant and the value of N_{max} for this process (presumably driven by the dimensions of the molecule and thus likely to be in the range of 10^{14} molecules per cm^2) are both not known. As is obvious from the

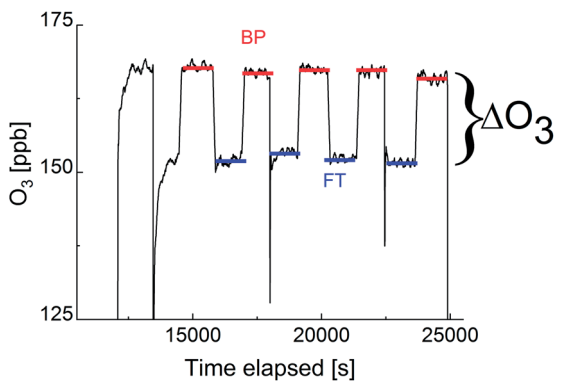

Fig. 2 An example of the O_3 mixing ratio measured downstream of the flow tube in response to switching the gas flow from the bypass (BP, red lines) to the injector and thus, through the coated wall flow tube (FT, blue lines). Experiments were done at 5 °C with an activity of Br^- of 0.58 M and of citric acid of 0.08 M.

present data set and also from others discussed further below, there are no indications so far that the adsorption saturation of O_3 on water affects surface to bulk transfer.

The parameterization for Γ_{bulk} (eqn (5)) contains temperature-dependent parameters (Henry's law constant (H), diffusivity (D_{O_3}), the mean thermal velocity of O_3 (ω_{O_3}), and the *pseudo*-first order bulk aqueous phase rate coefficient ($k_b^I = k_b^{II} \times a_{[Br^-]}$ ($a_{[Br^-]}$ is bromide activity)). R is the ideal gas constant. There is limited information on the aforementioned parameters and their temperature dependences. In cases where there are measurement data, these are often conducted for single solute solutions not below 0 °C. Therefore, we have parameterized these factors for ternary mixtures and lower temperatures as described below.

Results and discussion

In Fig. 3, we present the measured uptake coefficients (γ_{obs}) corrected for the gas phase diffusion limitation of O_3 in the in the mixed citric acid/NaBr solutions as a function of temperature from −25 °C to 16 °C. The observed temperature dependence shows that uptake coefficients of ozone decrease with decreasing temperature. This decrease slows down and plateaus below −10 °C. The observed uptake coefficients at −20 °C and −25 °C are invariant. The uptake coefficients observed in our study were about 1×10^{-7} at −20 °C with 3×10^{13} molecules per cm^3 ozone concentration which compares well with that of Oldridge and Abbatt's study on acidic ternary mixtures of NaCl, NaBr, and water.[40] The concentration of the condensed phase reactant in both studies is determined by the freezing point depression at temperatures below 0 °C (Fig. 1). Thus the agreement of the observed uptake coefficients for this particular run with similar experimental conditions supports the finding of the earlier study. The comparison is, however, hampered by the presence of citric acid in our study. In this study, we have extended the temperature range and in particular increased the sampling interval to investigate the multiphase reactivity in more detail. As described below, there are distinct differences in observed uptake coefficients as a function of ozone concentrations between the studies.

In Fig. 3, we also present three predictions of the uptake coefficients (γ_{calc}, lines) as a function of temperature. The runs differ in the parameterization of the diffusivity of ozone and the ozone solubility in the film. The grey line denotes a run where the diffusivity and the solubility of ozone in the reactive medium are parameterized without considering the effect of solutes on either. Such a parameterization based on the diffusivity of ozone[54] and ozone solubility in water[55] does not capture the observations. In particular, the marked increase in the uptake coefficient at 273 K, when water activity decreases leading to an increase in bromide activity (Fig. 1), is not evident in the experimental data. The agreement between the parameterization output and the observations is drastically improved, when accounting for the impact of bromide on the solution's properties. Finally, incorporating the effect of the organic solute as well further optimizes the parameterization result showing the importance of accurately describing the physical properties of organic–inorganic mixtures. The relevant film properties and parameters such as the viscosity and diffusivity of ozone, solubility of ozone in the film, pH of the film, and rate of the reaction in the aqueous bulk are developed further below and summarized in Table 1 and ESI Tables S1–S3.†

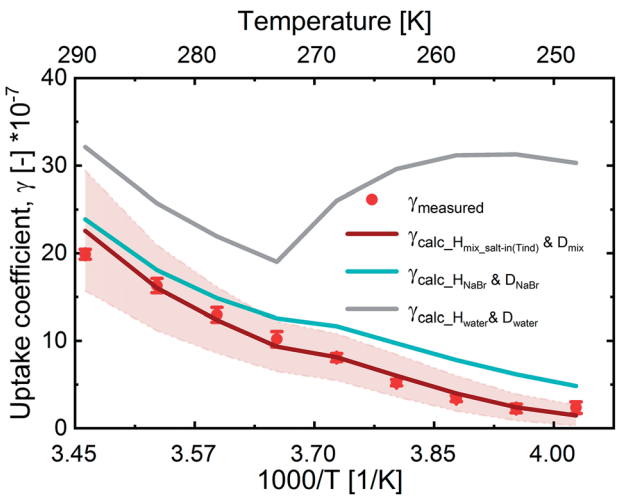

Fig. 3 Measured (dots) and parameterized (lines) uptake coefficients as a function of temperature at 5×10^{12} molecules per cm^3 ozone concentration. The grey line parameterization uses the solubility and diffusivity of ozone in water. The cyan line uses the diffusivity and solubility in a solution containing the film's concentration of NaBr, but not citric acid. The red line uses the diffusivity and solubility of ozone as estimated for both NaBr and citric acid. The reaction rate coefficients are the same for all three runs. The red shaded area denotes the standard deviation (s.d.) of multiple repeats.

Aqueous bulk reaction rate coefficients

One parameter of Γ_{bulk} is the *pseudo*-first order rate coefficient for the reaction of ozone with bromide (k_b^I, eqn (5)) which is the product of the activity of bromide (a_{Br^-}) and the second-order rate coefficient (k_b^{II}). The activities and concentrations of the bromide and citric acid solutes were calculated using the AIOMFAC model, web version 2.18.[49] The mass fractions calculated using the AIOMFAC model for the binary water–bromide and water–citric acid systems, respectively, compare well with that obtained using freezing point depression data for NaBr[14] and growth factors for citric acid.[56] To convert the AIOMFAC output to activities based on molarity as required for the kinetics description, the density of the film was estimated using the mass fraction (of dry solute) mixing rule of the individual solutes and their solutions. The density of the citric acid solution was determined using the parameterization proposed by Lienhard *et al.*[17] The density of the NaBr solution was estimated by extrapolating measurements of Isono.[57]

The second order rate coefficient for the reaction of Br^- with O_3 (eqn (6)) is based on the mechanism presented in R1–R5, and is pH dependent.[32]

$$k_b^{II} = \frac{k_1\left(\frac{k_2}{k_{-1}}[H^+] + \frac{k_3}{k_{-1}}\right)}{1 + \frac{k_2}{k_{-1}}[H^+] + \frac{k_3}{k_{-1}}} \quad (6)$$

Estimation of the pH of the film was based on citric acid dissociation constants and activity in the film.[58] The estimated pH ranged from ~2 at 16 °C to ~1.7 at −25 °C (Table 1). The temperature dependence of k_b^{II} was a free tuning parameter benchmarked against the pH independent rate coefficient involving R3 but not R2 ($k_{H_2O} = k_1/((k_{-1}/k_3) + 1)$) proposed by Liu *et al.*, 258 M^{-1} s^{-1} at 25 °C.[32] This study's parameterized k_b^{II} at 16 °C was 388 M^{-1} s^{-1}. The calculated k_b^{II} with our own fit at 25 °C and 1 M H^+ is 1.7×10^3 M^{-1} s^{-1}, which is much smaller than that calculated by Liu *et al.* at 25 °C, 3.64×10^3 M^{-1} s^{-1}.[32] The pH independent rate coefficient, which was used as a benchmark, from our parameterization is 257 M^{-1} s^{-1} at 25 °C and, like that of Liu *et al.*, is larger than that of Haruta and Takeyama (211 M^{-1} s^{-1} at 27 °C[33]) and Haag and Hoigné (206 M^{-1} s^{-1} at 25 °C at pH 2).[59]

This comparison illustrates the uncertainty in the present second order rate coefficients and their temperature dependence, which is directly reflected in the uncertainty of k_b^I. Further uncertainty in the *pseudo*-first order rate coefficients arises from the uncertainties in the activity coefficients as derived from the AIOMFAC model, the density estimates for the film, and the pH of the film (ESI Table S4†). We have assigned about 20% (35%) uncertainty to this parameter at temperatures above 0 °C (at −20 °C) taking the aforementioned sources of errors into consideration. A 22% change in the *pseudo*-first order rate coefficient at 0 °C results in a 9% change in the γ_{calc} and a 34% change in the rate coefficient at −20 °C results in a 16% change in the γ_{calc} (Table 2).

Overall, the increase in $\gamma_{calc\_Hwater\_Dwater}$ following the trend in bromide activity with temperature is in line with a concentration driven acceleration of apparent reaction rates observed in other bimolecular (or higher-order) reactions.[5] Fig. 3 shows that other factors reduce the apparent reactivity in this multiphase system, which we will discuss in the following.

Ozone solubility in the aqueous bulk

Fig. 3 shows the profound influence of composition driven equilibrium partitioning of ozone between the gas phase and the aqueous bulk on Γ_{bulk} (eqn (5)). This is a well-known effect;[60,61] however, there are no data quantifying these effects at the high molarities and at the low temperatures typical for atmospheric chemistry. Here, we present and test approaches to overcome this limitation.

Table 2 Uncertainty and sensitivity of Γ_{bulk} and γ_{calc} to solubility (H_{mix}), diffusivity of ozone ($D_{O_{3l}\_mix}$), and the rate of reaction in the aqueous bulk (k_b^I)

	H_{O_3Mix}			$D_{O_{3l}\_mix}$			k_b^I		
T [°C]	16	0	−20	16	0	−20	16	0	−20
% Uncertainty applied	20	20	35	5	5	9	22	22	34
% Change in Γ_{bulk}	19	20	34	3	2	4	11	11	17
% Change in γ_{calc}	12	17	32	2	2	4	7	9	16

The effect of solutes on solubility is referred to as "*Salting*," which may be *salting-out* or *salting-in* and is described with the so-called "Sechenov relationship" (eqn (7)).[60–64]

$$\log(H_{solution}/H_{water}) = K_s a_s \quad (7)$$

$H_{solution}$ (mol (L atm)$^{-1}$) is Henry's law constant of ozone in the solution and K_s is the Sechenov constant. H_{water} is the Henry's law constant of ozone in water (mol (L atm)$^{-1}$; eqn (8)[55]). This treatment of the high ionic strength of bromide and high concentration of citric acid expands the use of the term, Henry's law constant, that strictly refers to the limiting case of gas-aqueous bulk partitioning for low ionic strength and solute concentrations.

$$H_{water} = 0.0115 \times \exp\left(2560 \times \left(\frac{1}{T} - \frac{1}{298}\right)\right) \quad (8)$$

where T denotes the temperature.

In the presence of NaBr the ozone gas-aqueous bulk partitioning coefficient decreases significantly by ~30% above 0 °C with a stronger salting-out as NaBr concentrations increase with decreasing temperatures below 0 °C (Fig. 3). This is in agreement with the general trend for gases less polar than water, where inorganic salts tend to decrease gas solubility (a *salting-out* effect).[63,65] The solubility was derived using parameterizations of the Sechenov constants for NaBr solutions as described by Weisenberger and Schumpe.[65] These parameterizations were done using data obtained above 0 °C.[64,65] Due to low confidence on the temperature dependence as expressed by the authors,[65] we fixed it to that at 25 °C.[64]

Additional incorporation the effect of the organic co-solute on Γ_{bulk} leads to a perfect agreement with the experimental data (Fig. 3). To achieve this, two scenarios estimating the solubility of O_3 in the aqueous citric acid solution were developed as part of this study. On the one hand, we described the *salting* effect of citric acid as that typical for organic species, for which a *salting-*

Table 1 Film composition and properties at 16 °C, 0 °C and −20 °C[a]

T [°C]	$a_{[Br^-]}$ [M]	$a_{[CA]}$ [M]	pH	k_b^{II} [M^{-1} s^{-1}]	$D_{O_{3l}\_mix}$ [cm^2 s^{-1}]	$H_{mix\_salt\text{-}in(T\text{-}ind)}$ [mol (L atm)$^{-1}$]	O_3 [#/cm^{-3}]	k_s^I [s^{-1}]	K cm^3 per molecule
16	0.6	0.09	2.1	388	1.20×10^{-5}	9.94×10^{-3}	4.31×10^{12}	3.31×10^{-2}	6.43×10^{-12}
0	0.6	0.08	2.1	123	6.80×10^{-6}	1.40×10^{-2}	4.57×10^{12}	5.15×10^{-3}	7.38×10^{-12}
−20	3.8	0.5	1.7	25	5.70×10^{-7}	1.20×10^{-2}	4.93×10^{12}	3.61×10^{-4}	9.00×10^{-12}

[a] T is temperature; $a_{[Br^-]}$ is Bromide activity and $a_{[CA]}$ is citric acid activity (AIOMFAC calculations); k_b^{II} is second order bulk rate coefficient; D_{O3l} is O_3 diffusivity; H_{mix} is ozone solubility, k_s^I is the surface rate coefficient, K is the surface adsorption coefficient.

in effect with increasing concentration of the organic species is generally observed.[61] For this, we used measurements of O_3 solubility in propionic acid–water mixtures at room temperature between 0 weight percent and 100 weight percent propionic acid.[60] On the other hand, measurements of oxygen solubility in citric acid solutions at 25 °C indicate a *salting-out* effect with increasing citric acid concentrations (between 0.13 and 1.04 M citric acid).[66,67] Since O_3 solubility often follows similar dependences as that of O_2,[61] we consider this *salting-out* scenario as likely as the *salting-in*.

Fig. 4 presents the solubility for the aforementioned two scenarios. The *salting-in* scenario, $H_{O_3\_CAsalt\text{-}in}$, shows a strong increase of ozone solubility with decreasing temperature. This trend is driven by the temperature dependence of $H_{solution}$ that we set to that of H_{water}. Since we are uncertain about the temperature dependence of ozone solubility in this solution, we considered a second alternative to this *salting-in* scenario, where the solubility has no temperature dependence and the small trend in Fig. 4 is only caused by the change in citric acid concentration.

The *salting-out* scenario, $H_{O_3\_CAsalt\text{-}out}$, shows a similar temperature dependence to H_{O_3NaBr} with an increase in solubility with decreasing temperature, a decrease at 0 °C as concentrations increase and a further increase as the temperature effect dominates again. $H_{O_3CA\_salt\text{-}out}$ is significantly lower than H_{water}. The solubility of O_3 in the film mixture (H_{O_3Mix}) was calculated by applying the volume mixing rule to the three scenarios for the citric acid fraction and the solubility in the NaBr fraction, H_{O_3NaBr} (eqn (9)).

In summary, the solubility in the different fractions shows an increase with decreasing temperature up to 0 °C. Below 0 °C, there is a discontinuity (except in $H_{O_3\_CAsalt\text{-}in}$ and $H_{O_3\_CAsalt\text{-}in(T\text{-}ind)}$) due to the effect of increasing solute concentrations with decreasing water activity as temperatures decrease. All mixture scenarios (H_{O_3Mix}) show an overall *salting-out* effect; that is, H_{O_3Mix} is less than H_{water}. The discontinuity at 0 °C in the fractions is also reflected in the H_{O_3Mix}.

$$H_{O_3Mix} = Volfrac_{NaBr} \cdot H_{O_3NaBr} + Volfrac_{CA} \cdot H_{O_3CA} \quad (9)$$

Fig. 5 shows an assessment of the impact of the different solubility scenarios on the uptake coefficients, with all other factors remaining the same. The γ_{calc} for the *salting-in* scenario with $H_{O_3\_CAsalt\text{-}in}$, $\gamma_{HO_3Mix\_salt\text{-}in}$, does not concur with the observed uptake coefficients below 0 °C. This indicates that the rather strong temperature dependence described by the temperature dependence of H_{O_3water} poorly represents the temperature dependence of O_3 solubility with the *salting*-in effect. This observation is in agreement with the small general temperature dependence found in the *salting* effect of the organic co-solute.[68] Decoupling the temperature dependence of the solubility effect of the organic fraction from that of water gives better results ($\gamma_{HO_3Mix\_CAsalt\text{-}in(T\text{-}ind)}$ and $\gamma_{HO_3Mix\_CAsalt\text{-}out}$).

The difference between these two scenarios calls for further studies on gas solubility in organic mixtures at low temperatures. In general, due to the absence of measurements of ozone solubility in organic–inorganic mixtures at temperatures below 0 °C, there are large uncertainties. We have estimated this uncertainty based on the difference between the different scenarios (ESI Table S4†). A 20% change in the solubility parameter at 0 °C resulted in a 12% change in the γ_{calc} and

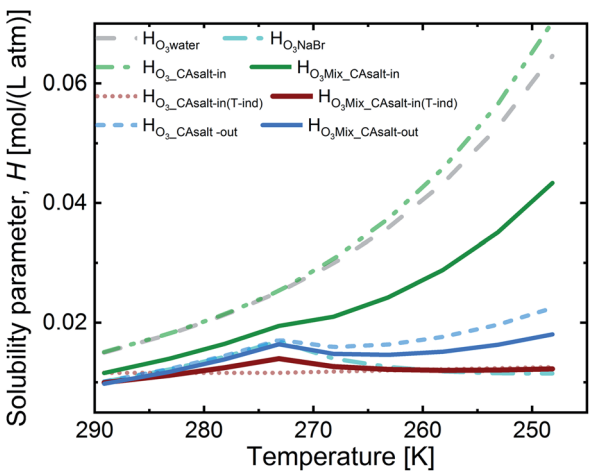

Fig. 4 Calculated ozone solubility in solution fractions and in the mixture (by the volume mixing rule). H_{O_3i} is Henry's law O_3 solubility in solution (i). Grey dashed line: H_{O_3water}; cyan dash-dot line: H_{O_3NaBr}; green-dash-dot-dot line: $H_{O_3\_CAsalt\text{-}in}$, *salting-in* effect with T dependence of H_{O_3water}; red dotted line: $H_{O_3\_CAsalt\text{-}in(T\text{-}ind)}$, *salting-in* effect without T-dependence; blue dashed line: $H_{O_3\_CAsalt\text{-}out}$, *salting-out* effect with T dependence of H_{O_3water}; *solid green* line: $H_{O_3Mix\_CAsalt\text{-}in}$ with $H_{O_3\_CAsalt\text{-}in}$; *solid red* line: $H_{O_3Mix\_CAsalt\text{-}in(T\text{-}ind)}$ with $H_{O_3\_CAsalt\text{-}in(T\text{-}ind)}$, *solid blue* line: $H_{O_3Mix\_CAsalt\text{-}out}$ with $H_{O_3\_CAsalt\text{-}out}$; all H_{O_3Mix} contain volume ratio combinations of the $H_{O_3\_CA}$ scenarios and H_{O_3NaBr} surface reaction.

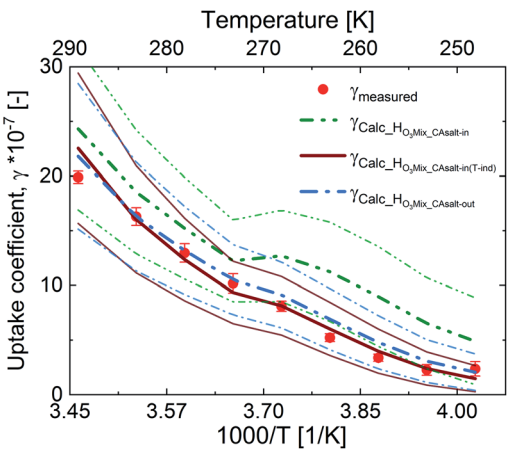

Fig. 5 Measured (dots) and parameterized (lines) uptake coefficients as a function of temperature at 5×10^{12} molecules per cm^3 ozone concentration. The parameterizations differ with the ozone solubility in the presence of citric acid: The dash-dot-dot green line is the parameterization with the salting-in effect of the organic with the temperature dependence of O_3 solubility in water + salting-out effect of NaBr; the solid red line is the parameterization with the salting-in effect of the organic without the temperature dependence of O_3 solubility in water + salting-out effect of NaBr; the dash-dot blue line is the parameterization with the salting-out effect of the organic with the temperature dependence of O_3 solubility in water + *salting-out* effect of NaBr. The thin lines are error bands for the output.

a 35% change in the solubility parameter resulted in a 32% change in γ_{calc} at −20 °C (Table 2).

In summary, both $H_{O_3Mix\_CAsalt\text{-}in(Tind)}$ and $H_{O_3Mix\_CAsalt\text{-}out}$ give good results and can be used to assess ozone solubility in mixed systems at temperatures below the freezing point of water.

Viscosity and aqueous bulk diffusivity of ozone

The excellent agreement between γ_{calc} and γ_{obs} in Fig. 3 was also achieved by parameterizing the diffusivity in the film. The viscosity of the film influences the diffusivity of ozone and the products within the film. The diffusivity of ozone in the film was estimated using the Stokes–Einstein relationship (eqn (10)), in which diffusivity is inversely related to viscosity. The Stokes–Einstein relationship is valid for small molecules and viscosities lower than 10 Pa s.[69] The viscosity of the film was obtained by measuring the viscosity of the solutions at the equilibrium concentrations, as calculated by AIOMFAC, at each experimental temperature. The viscosity of the film increased from 1.4 mPa s at 16 °C to 43.9 mPa s at −24 °C, which leads to almost a 40 times decrease in diffusivity. The measured viscosity of the mixture is similar to that measured in citric acid solutions.[70] Therefore, this increase in viscosity with decreasing T and increasing concentration is predominantly driven by citric acid (ESI Fig. S3†).[14,71]

$$D_{O_{3l}} = \frac{k_B T}{6\pi\eta(T) r_{O_3}} \quad (10)$$

Γ_{bulk} as presented in eqn (5) above is applicable if the reacto-diffusive length (l_{rd}) is smaller than the thickness of the film (t_{film}). In this case, the uptake in the aqueous bulk is limited by both reaction and diffusion in the aqueous bulk. The l_{rd} is defined as the characteristic distance over which the reactant (O_3) is lost due to reaction in the film (eqn (11)).[51]

$$l_{rd} = \sqrt{\frac{D_{O_{3l}}}{k_b^I}} \quad (11)$$

If the l_{rd} is almost equal to or larger than the t_{film}, the reaction occurs almost throughout the depth or thickness of the film; Γ_{bulk} will be proportional to the volume of the film (or thickness). The thickness of the film was obtained by dividing the estimated volume of the film by the internal surface area of the tube (188.5 cm^2). The film thickness ranged from ∼2 μm at −25 °C to ∼13 μm at 16 °C while the l_{rd} ranged from 0.7 μm at −25 °C to 2.3 μm at 16 °C. Hence, we assumed that eqn (5) is a good representation of Γ_{bulk}.

We have assigned a low uncertainty to the diffusivity parameter due to the viscosity measurements for the equilibrium concentrations of solutes in the film, which were conducted as part of this study. The equilibrium concentrations calculated using the AIOMFAC model may also be a source of uncertainty for this parameter. A 5% change in the diffusivity parameter at 0 °C results in a 2% change in γ_{calc} and a 10% change in the diffusivity at −20 °C results in a 4% change in γ_{calc} (Table 2).

Uncertainty in aqueous bulk properties and impact on γ_{calc}

Although we are able to predict the measured uptake coefficients in this system, there are uncertainties in the parameters. The uncertainties arise from the lack of measurements of the parameters for the organic component and mixture in particular below 0 °C. Therefore, extrapolation to lower temperatures comes with large uncertainties. Fig. 5 shows the γ_{calc} with error bands (thinner lines). The error bands were determined *via* error propagation with increasing percentage error as temperatures decreased below 0 °C for all surface and bulk parameters.

Table 2 presents a summary of the uncertainties in the bulk parameters and their implications on the bulk uptake coefficients and total uptake coefficients at 16 °C, 0 °C, and −20 °C. Uncertainties in all parameters increase as temperatures decrease below 0 °C due to the absence of measurements and parameterizations at colder temperatures and high concentrations. ESI Table S4† contains information on uncertainties assigned to each parameter and at different temperatures. In summary, the bulk uptake coefficients and the total uptake coefficients are most sensitive to the solubility parameter. The solubility parameter is also the largest source of uncertainty.

Fig. 6 presents the measured uptake coefficients as a function of ozone concentration at 0 °C, −10 °C, −20 °C and −25 °C, also corrected for the gas phase diffusion limitation. The uptake coefficients were independence of ozone concentration at 0 ° and −10 °C. At temperatures less than −10 °C, this independence occurs only at high ozone concentrations. That the uptake coefficient is invariant with increasing ozone concentration shows that Γ_{bulk} is not limited by the uptake of ozone from the gas phase. Only at higher ozone concentrations, the surface to bulk transfer rate may be limited by saturation in surface coverage.[40,52] There is some evidence of negative O_3 concentration dependence at −20 °C and −25 °C, but not at higher temperatures. At −20 and −25 °C, the uptake coefficients decrease with increasing ozone concentration and then plateau to a constant value at high O_3 concentrations. This negative O_3 concentration dependence of the uptake coefficient is the result of the saturation of the surface coverage of the bromide ozonide occurring at ozone concentrations below those employed here. This observation is different from that of Oldridge and Abbatt with 8.6 mM NaBr concentration at 0 °C,[40] and Artiglia *et al.* with 0.12 M and 0.24 M NaBr concentration at 1 °C[41] where a negative O_3 concentration dependence was observed. Considering that bromide was 0.7 M at 0 °C in the study presented here, the absence of O_3 concentration dependence is not linked to the bromide concentration.

The uptake coefficients at −20 °C and −25 °C are essentially the same. This observation is similar to the levelling off with temperature observed by Oldridge and Abbatt below −30 °C in their system without organics.[40] This plateauing in temperature dependence at a warmer temperature in our study may be due to the presence of the organic component. Due to the increase in viscosity with temperature (and concentration of the organic species), the decrease in the diffusivity may lower the contribution of the aqueous bulk to the total O_3 uptake; hence similar

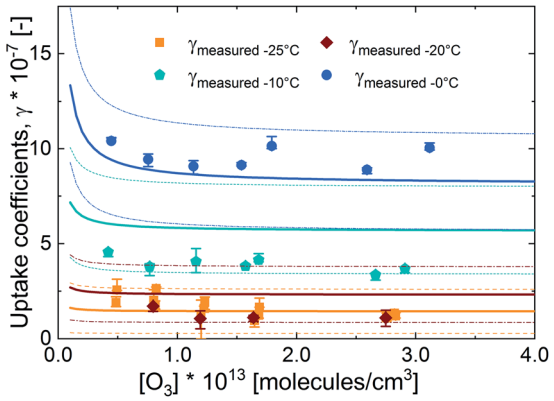

Fig. 6 Measured and parameterized uptake coefficients ($H_{O_3Mix\_CAsalt\text{-}in(T\text{-}ind)}$) with error bands at different temperatures as a function of gas-phase ozone concentration. The dots are the measured uptake coefficients; the solid lines are the model lines; the thin dashed lines are the error bands for the parameterization output. The parameterization output and error bands have the same colour as the temperature in question: *blue circles* ● for 0 °C, *cyan pentagons* ⬟ for −10 °C, *red diamonds* ◆ for −20 °C, and *orange squares* ■ for −25 °C.

total uptake coefficients are observed. These conditions may also increase the potential for surface uptake.

The parameterization output, also presented in Fig. 6, was able to predict the O_3 concentration dependence of the uptake coefficients reasonably well. At −20 °C, the parameterization is not able to capture the observed similarity in the uptake coefficients between −20 °C and −25 °C. This may be due to uncertainties in the solubility parameter at low temperatures and higher viscosity as well as uncertainties in the surface uptake parameters.

The surface uptake parameterization used in this study was that developed by Artiglia *et al.* for a system without organics.[41] This may not be ideal for the mixed matrix in this study, where the partitioning of the solutes to the surface may not be the same as in a single solute solution.[20–22] In particular, recent X-ray photoelectron spectroscopy data of Lee *et al.* have demonstrated that the presence of citric acid led to a reduction of the bromide abundance at the solution–air interface.[22] In addition, the temperature dependence of the surface rate coefficient, k_s, may be different in this study due to the presence of organics. The k_s from Artiglia *et al.* applied in this study was based on the energy difference between the water stabilized surface intermediate, $BrOOO^- \cdot 4H_2O$ and the transition state species after intersystem crossing in the reaction scheme on the surface.[41] The organics present on the surface may influence the stabilization of this intermediate, as citric acid is a good ligand, with impacts on the k_s.

The γ_{calc} is quite sensitive to the magnitude of N_{max} and k_s in eqn (4). An increase in k_s by a factor of 10 increases γ_{calc} by a factor of 4.3 at 16 °C and 1.25 at −25 °C. An increase in N_{max} by a factor of 10 increases γ_{calc} by a factor of 2.2 at 16 °C and 1.1 at −25 °C. γ_{calc} is partly sensitive to K with a maximum of about 2% increase with an increase by a factor of 10. Increasing K increases surface coverage of the intermediate ozonide. Since the parameterization of the surface uptake coefficients is already close to the maximum surface coverage, there is no significant change with an increase in K. A decrease in K by a factor of 10 decreases γ_{calc} at warmer temperatures by about 8% due to a significant decrease in surface coverage at warmer temperatures. At temperatures below 0 °C, the change (increase) is about 1% due to a much weaker effect on the surface coverage. This is due to the temperature dependence of K.

In summary, the data indicate a surface process at low temperatures (−20 °C and −25 °C) and low ozone concentrations. The lower surface adsorption equilibrium constant and lower coverage at warmer temperatures result in lower contributions from the surface reaction. At colder temperatures, the coverage is higher, but the surface reaction rate coefficients are lower. The parameterization indicates a significant surface process at ozone concentrations lower than the experimental range. We attribute this difference to uncertainties in k_s and K, and their temperature dependence.

Conclusions and implications

In this study, we measured the temperature dependence of the dark reaction of O_3 with bromide in a proxy for sea-spray aerosols and brine on sea-ice and in snow. This proxy contained a mixture of an organic species and an inorganic salt (citric acid and sodium bromide). A decrease in temperature resulted in a significant increase in the concentration of solutes below 0 °C as the water vapour pressure decreased. This further resulted in an increase in the *pseudo*-first order rate coefficients.

For this mixed system with organics, a combination of increased viscosity and a strong decrease in the solubility of ozone due to increase in the concentrations of the solutes countered the reaction acceleration. Increased viscosity due to the increased concentration of citric acid with decreasing temperature led to a significant decrease in diffusivity. Sea-spray aerosols and brine on environmental ice surfaces such as snow and sea ice contain a significant organic component, which may strongly influence their viscosity.[16,19] This effect of citric acid on the viscosity and on the uptake of O_3 in this study is in agreement with that in other studies, which have shown similar reduced reactivity due to the impact of high viscosity on heterogeneous reactions.[23,24] We note, though, that the viscosity effect seen here becomes relevant even at high relative humidity, as it is common for environmental compartments where brine is in equilibrium with ice. This effect has implications for the reaction of halides with O_3 in snow covered Arctic sea-ice where a significant source of salinity on surface snow is sea-spray aerosols,[3] and where aged organic species (represented by citric acid in this study) are likely co-located with halide ions.[3,30]

There is limited information on the solubility of O_3 and other oxidants in organic solutions and in organic/inorganic mixtures although O_3 is one of the important oxidants in the atmosphere. The heterogeneous reactions of O_3 in aerosols or brine pockets, which contain complex mixtures of solutes, may not be properly assessed without properly accounting for the concentration of O_3 in the condensed phase. From our solubility calculations, the composition of the mixture resulted in a significant *salting-out* effect on O_3 relative to O_3 solubility in water; using the solubility of O_3 in water overestimates the uptake coefficients.

Based on our results, atmospheric models may simply be able to use a general representation of the *salting* effect of solutes on the solubility of the reacting gas.

Halogen activation *via* reaction between O_3 and halides in sea-spray aerosols has recently been updated in global atmospheric chemistry models.[7] The addition of the multiphase chemistry contribution from sea-spray aerosols has been shown to improve model predictions. These models may be further improved by including some information about the average viscosity of sea-spray aerosols and the composition effect on solubility. This implies that there is a need for measurements of solubility of O_3 in mixtures which is presently lacking. Recently, there have been more studies measuring the viscosity of sea-spray aerosol.[19]

In addition, we did not focus on the surface uptake of ozone in the mixture as part of this study. There is increasing knowledge of significant surface contributions to the uptake of O_3 in aerosols at lower, atmospherically relevant O_3 concentrations. Organics have been shown to influence the partitioning of the halides to the surface[21,22] and the reactivity on the surface.[20] Further studies at low ozone concentrations on the influence of organics and mixtures on the surface uptake of ozone is needed for information on the surface uptake parameters such as the surface rate coefficients, the surface adsorption coefficients, and the maximum coverage of the reactants on the surface (N_{max}). The total uptake coefficients are particularly sensitive to the N_{max} and the surface rate coefficients.

Conflicts of interest

There are no conflicts to declare.

Acknowledgements

The authors would like to thank Mario Birrer for assistance in building the experimental set-up. This project was funded by the Swiss National Foundation (grant number 155999).

Notes and references

1 W. R. Simpson, R. von Glasow, K. Riedel, P. Anderson, P. Ariya, J. Bottenheim, J. Burrows, L. J. Carpenter, U. Friess, M. E. Goodsite, D. Heard, M. Hutterli, H. W. Jacobi, L. Kaleschke, B. Neff, J. Plane, U. Platt, A. Richter, H. Roscoe, R. Sander, P. B. Shepson, J. Sodeau, A. Steffen, T. Wanger and E. Wollf, *Atmos. Chem. Phys.*, 2007, **7**, 4375–4418.

2 W. R. Simpson, S. S. Brown, A. Saiz-Lopez, J. A. Thornton and R. Glasow, *Chem. Rev.*, 2015, **115**, 4035–4062.

3 J. P. D. Abbatt, J. L. Thomas, K. Abrahamsson, C. Boxe, A. Granfors, A. E. Jones, M. D. King, A. Saiz-Lopez, P. B. Shepson, J. Sodeau, D. W. Toohey, C. Toubin, R. von Glasow, S. N. Wren and X. Yang, *Atmos. Chem. Phys.*, 2012, **12**, 6237–6271.

4 M. Nerentorp Mastromonaco, K. Gårdfeldt, B. Jourdain, K. Abrahamsson, A. Granfors, M. Ahnoff, A. Dommergue, G. Méjean and H. W. Jacobi, *Atmos. Environ.*, 2016, **129**, 125–132.

5 T. Bartels-Rausch, H. W. Jacobi, T. F. Kahan, J. L. Thomas, E. S. Thomson, J. P. D. Abbatt, M. Ammann, J. R. Blackford, H. Bluhm, C. Boxe, F. Domine, M. M. Frey, I. Gladich, M. I. Guzmán, D. Heger, T. Huthwelker, P. Klán, W. F. Kuhs, M. H. Kuo, S. Maus, S. G. Moussa, V. F. McNeill, J. T. Newberg, J. B. C. Pettersson, M. Roeselová and J. R. Sodeau, *Atmos. Chem. Phys.*, 2014, **14**, 1587–1633.

6 M. S. Long, W. C. Keene, R. C. Easter, R. Sander, X. Liu, A. Kerkweg and D. Erickson, *Atmos. Chem. Phys.*, 2014, **14**, 3397–3425.

7 J. A. Schmidt, D. J. Jacob, H. M. Horowitz, L. Hu, T. Sherwen, M. J. Evans, Q. Liang, R. M. Suleiman, D. E. Oram, M. Le Breton, C. J. Percival, S. Wang, B. Dix and R. Volkamer, *J. Geophys. Res.: Atmos.*, 2016, **121**, 11819–11835.

8 S. Wang, J. A. Schmidt, S. Baidar, S. Coburn, B. Dix, T. K. Koenig, E. Apel, D. Bowdalo, T. L. Campos, E. Eloranta, M. J. Evans, J. P. DiGangi, M. A. Zondlo, R. S. Gao, J. A. Haggerty, S. R. Hall, R. S. Hornbrook, D. Jacob, B. Morley, B. Pierce, M. Reeves, P. Romashkin, A. Ter Schure and R. Volkamer, *Proc. Natl. Acad. Sci. U. S. A.*, 2015, **112**, 9281–9286.

9 P. K. Peterson, D. Pöhler, H. Sihler, J. Zielcke, S. General, U. Frieß, U. Platt, W. R. Simpson, S. V. Nghiem, P. B. Shepson, B. H. Stirm, S. Dhaniyala, T. Wagner, D. R. Caulton, J. D. Fuentes and K. A. Pratt, *Atmos. Chem. Phys.*, 2017, **17**, 7567–7579.

10 F. Dominé, R. Sparapni, A. Ianniello and H. J. Beine, *Atmos. Chem. Phys.*, 2004, **4**, 2259–2271.

11 T. Koop, A. Kapilashrami, L. T. Molina and M. J. Molina, *J. Geophys. Res.*, 2000, **105**, 26393–26402.

12 H. Cho, P. B. Shepson, L. A. Barrie, J. P. Cowin and R. Zaveri, *J. Phys. Chem. B*, 2002, **106**, 11226–11232.

13 N. Takenaka, U. Akihiro and M. Yasuaki, *Nature*, 1992, **358**, 736–738.

14 Concentrative properties of aqueous solutions: density, refractive index, freezing point depression, and viscosity, in *CRC Handbook of Chemistry and Physics*, ed. J. R. Rumble, CRC Press/Taylor & Francis, Boca Raton, FL, 2018.

15 R. O'Concubhair and J. R. Sodeau, *Environ. Sci. Technol.*, 2012, **46**, 10589–10596.

16 C. D. O'Dowd, M. C. Facchini, F. Cavalli, D. Cebrunis, M. Mircea, S. Decesari, S. Fuzzi, Y. J. Yoon and J.-P. Putaud, *Nature*, 2004, **431**, 672–676.

17 D. M. Lienhard, D. L. Bones, A. Zuend, U. K. Krieger, J. P. Reid and T. Peter, *J. Phys. Chem. A*, 2012, **116**, 9954–9968.

18 J. P. Reid, B. J. Dennis-Smither, N. O. Kwamena, R. E. Miles, K. L. Hanford and C. J. Homer, *Phys. Chem. Chem. Phys.*, 2011, **13**, 15559–15572.

19 J. P. Reid, A. K. Bertram, D. O. Topping, A. Laskin, S. T. Martin, M. D. Petters, F. D. Pope and G. Rovelli, *Nat. Commun.*, 2018, **9**, 956.

20 S. Hayase, A. Yabushita, M. Kawasaki, S. Enami, M. R. Hoffmann and A. J. Colussi, *J. Phys. Chem. A*, 2011, **115**, 4935–4940.

21 J. Werner, M. Dalirian, M. M. Walz, V. Ekholm, U. Wideqvist, S. J. Lowe, G. Ohrwall, I. Persson, I. Riipinen and O. Bjorneholm, *Environ. Sci. Technol.*, 2016, **50**, 7434–7442.

22 M. T. Lee, M. A. Brown, S. Kato, A. Kleibert, A. Turler and M. Ammann, *J. Phys. Chem. A*, 2015, **119**, 4600–4608.
23 S. S. Steimer, M. Lampimäki, E. Coz, G. Grzinic and M. Ammann, *Atmos. Chem. Phys.*, 2014, **14**, 10761–10772.
24 F. H. Marshall, R. E. H. Miles, Y. C. Song, P. B. Ohm, R. M. Power, J. P. Reid and C. S. Dutcher, *Chem. Sci.*, 2016, **7**, 1298–1308.
25 L. Renbaum-Wolff, J. W. Grayson, A. P. Bateman, M. Kuwata, M. Sellier, B. J. Murray, J. E. Shilling, S. T. Martin and A. K. Bertram, *Proc. Natl. Acad. Sci. U. S. A.*, 2013, **110**, 8014–8019.
26 D. Toom-Sauntry and L. A. Barrie, *Atmos. Environ.*, 2002, **36**, 2683–2693.
27 D. L. Mitchell and D. Lamb, *J. Geophys. Res.*, 1989, **94**, 14831–14840.
28 V. F. McNeill, A. M. Grannas, J. P. D. Abbatt, M. Ammann, P. Ariya, T. Bartels-Rausch, F. Domine, D. J. Donaldson, M. I. Guzman, D. Heger, T. F. Kahan, P. Klán, S. Masclin, C. Toubin and D. Voisin, *Atmos. Chem. Phys.*, 2012, **12**, 9653–9678.
29 A. M. Grannas, W. C. Hockaday, P. G. Hatcher, L. G. Thompson and E. Mosley-Thompson, *J. Geophys. Res.*, 2006, 111.
30 A. M. Grannas, A. R. Bausch and K. M. Mahanna, *J. Phys. Chem. A*, 2007, **111**, 11043–11049.
31 K. W. Oum, M. J. Lakin and B. J. Finlayson-Pitts, *Geophys. Res. Lett.*, 1998, **25**, 3923–3926.
32 Q. Liu, L. M. Schurter, C. E. Muller, S. Aloiso, J. S. Francisco and D. W. Margerum, *Inorg. Chem.*, 2001, **40**, 4436–4442.
33 K. Haruta and T. Takeyama, *J. Phys. Chem.*, 1981, **85**, 2383–2388.
34 Y. Sakamoto, M. Goda and J. Hirokawa, *J. Phys. Chem. A*, 2018, **122**, 2723–2731.
35 J. Liao, L. G. Huey, D. J. Tanner, F. M. Flocke, J. J. Orlando, J. A. Neuman, J. B. Nowak, A. J. Weinheimer, S. R. Hall, J. N. Smith, A. Fried, R. M. Staebler, Y. Wang, J. H. Koo, C. A. Cantrell, P. Weibring, J. Walega, D. J. Knapp, P. B. Shepson and C. R. Stephens, *J. Geophys. Res.: Atmos.*, 2012, **117**, 1–11.
36 J. P. Abbatt, *Geophys. Res. Lett.*, 1994, **21**, 665–668.
37 S. Fickert, J. W. Adams and J. N. Crowley, *J. Geophys. Res.*, 1999, **104**, 23719.
38 E. K. Frinak and J. P. Abbatt, *J. Phys. Chem.*, 2006, **110**, 10456–10464.
39 S. W. Hunt, M. Roeselová, W. Wang, L. M. Wingen, E. M. Knipping, D. J. Tobias, D. Dabdub and B. J. Finlayson-Pitts, *J. Phys. Chem. A*, 2004, **108**, 11559–11572.
40 N. W. Oldridge and J. P. Abbatt, *J. Phys. Chem. A*, 2011, **115**, 2590–2598.
41 L. Artiglia, J. Edebeli, F. Orlando, S. Chen, M.-T. Lee, P. Corral Arroyo, A. Gilgen, T. Bartels-Rausch, A. Kleibert, M. Vazdar, M. Andres Carignano, J. S. Francisco, P. B. Shepson, I. Gladich and M. Ammann, *Nat. Commun.*, 2017, **8**, 700.
42 S. N. Wren, T. F. Kahan, K. B. Jumaa and D. J. Donaldson, *J. Geophys. Res.*, 2010, 115.
43 A. Clifford and D. J. Donaldson, *J. Phys. Chem. A*, 2007, **111**, 9809–9814.
44 I. Gladich, J. S. Francisco, R. J. Buszek, M. Vazdar, M. A. Carignano and P. B. Shepson, *J. Phys. Chem. A*, 2015, **119**, 4482–4488.
45 K. Hebestreit, J. Stutz, D. Rosen, V. Matveiv, M. Peleg, M. Luria and U. Platt, *Science*, 1999, **283**, 55–57.
46 J. Marti and K. Mauersberger, *Geophys. Res. Lett.*, 1993, **20**, 363–366.
47 D. M. Murphy and T. Koop, *Q. J. R. Metereol. Soc.*, 2005, **131**, 1539–1565.
48 N. Takenaka and H. Bandow, *J. Phys. Chem. A*, 2007, **111**, 8780–8786.
49 A. Zuend, C. Marcolli, B. P. Luo and T. Peter, *Atmos. Chem. Phys.*, 2008, **8**, 4559–4593.
50 M. Ammann, R. A. Cox, J. N. Crowley, M. E. Jenkin, A. Mellouki, M. J. Rossi, J. Troe and T. J. Wallington, *Atmos. Chem. Phys.*, 2013, **13**, 8045–8228.
51 B. J. Finlayson-Pitts and J. N. J. Pitts, *Chemistry of the Upper and Lower Atmosphere*, Academic Press, San Diego California, USA, 2000.
52 U. Poschl, Y. Rudich and M. Ammann, *Atmos. Chem. Phys.*, 2007, **7**, 5989–6023.
53 M. Shiraiwa, C. Pfrang, T. Koop and U. Pöschl, *Atmos. Chem. Phys.*, 2012, **12**, 2777–2794.
54 P. N. Johnson and R. A. Davis, *J. Chem. Eng. Data*, 1996, **41**, 1485–1487.
55 W. L. Chaimedes and A. W. Stelson, *J. Geophys. Res.*, 1992, **97**, 20565–20580.
56 A. A. Zardini, S. Sjogren, C. Marcolli, U. K. Krieger, E. Weingartner, U. Baltensperger and T. Peter, *Atmos. Chem. Phys.*, 2008, **8**, 5589–5601.
57 T. Isono, *J. Chem. Eng. Data*, 1984, **29**, 45–52.
58 A. B. Hastings and D. D. V. Slyke, *J. Biol. Chem.*, 1922, **53**, 269–276.
59 R. W. Haag and J. Hoigné, *Environ. Sci. Technol.*, 1983, **17**, 261–267.
60 R. Battino, *Ozone Solubilities*, Pergamon Press Ltd, Oxford UK, 1981.
61 A. K. Biń, *Ozone: Sci. Eng.*, 2006, **28**, 67–75.
62 M. Sechenov, *Z. Phys. Chem.*, 1889, **4**, 117–125.
63 A. Schumpe, *Chem. Eng. Sci.*, 1993, **48**, 153–1158.
64 E. Rischbieter, H. Stein and A. Schumpe, *J. Chem. Eng. Data*, 2000, **45**, 338–340.
65 S. Weisenberger and A. Schumpe, *AIChE J.*, 1996, **42**, 298–300.
66 R. Battino, *Oxygen and Ozone - Solubility Data Series*, International Union of Pure and Applied Chemistry, 1981.
67 M. Popovic, H. Niebelschuetz and M. Reuss, *Eur. J. Appl. Microbiol. Biotechnol.*, 1979, **8**, 1–15.
68 D. D. Eley, *Trans. Faraday Soc.*, 1939, **35**, 1421–1432.
69 R. M. Power, S. H. Simpson, J. P. Reid and A. J. Hudson, *Chem. Sci.*, 2013, **4**, 2597.
70 D. M. Lienhard, A. J. Huisman, D. L. Bones, Y. F. Te, B. P. Luo, U. K. Krieger and J. P. Reid, *Phys. Chem. Chem. Phys.*, 2014, **16**, 16677–16683.
71 A. Apelblat, Properties of citric acid and its solutions, in *Citric Acid*, Springer, Cham, 2014, ch. 2, pp. 13–141, DOI: 10.1007/978-3-319-11233-6_2.